



UNIVERSITY OF LEEDS

This is a repository copy of *Design of an elbow for integrated gravimetric, electrochemical and acoustic emission measurements in erosion-corrosion pipe flow environments*.

White Rose Research Online URL for this paper:

<http://eprints.whiterose.ac.uk/143734/>

Version: Accepted Version

Article:

Owen, J, Ducker, E, Huggan, M et al. (3 more authors) (2019) Design of an elbow for integrated gravimetric, electrochemical and acoustic emission measurements in erosion-corrosion pipe flow environments. *Wear*, 428–429. pp. 76-84. ISSN 0043-1648

<https://doi.org/10.1016/j.wear.2019.03.010>

© 2019 Elsevier B.V. All rights reserved. This manuscript version is made available under the CC-BY-NC-ND 4.0 license <http://creativecommons.org/licenses/by-nc-nd/4.0/>.

Reuse

This article is distributed under the terms of the Creative Commons Attribution-NonCommercial-NoDerivs (CC BY-NC-ND) licence. This licence only allows you to download this work and share it with others as long as you credit the authors, but you can't change the article in any way or use it commercially. More information and the full terms of the licence here: <https://creativecommons.org/licenses/>

Takedown

If you consider content in White Rose Research Online to be in breach of UK law, please notify us by emailing eprints@whiterose.ac.uk including the URL of the record and the reason for the withdrawal request.

Design of an elbow for integrated gravimetric, electrochemical and acoustic emission measurements in erosion-corrosion pipe flow environments

Joshua Owen^a, Edward Ducker^a, Michael Huggan^a, Callum Ramsey^b, Anne Neville^a and Richard Barker^a

^a *Institute of Functional Surfaces, School of Mechanical Engineering, University of Leeds, Leeds, LS2 9JT, United Kingdom*

^b *Shell U.K. Limited, 1 Altens Farm Road, Nigg, Aberdeen, AB12 3FY, United Kingdom*

Abstract

Erosion-corrosion degradation in oil and gas pipelines is a significant problem, and a change in flow geometry can significantly enhance rates of degradation. In this study, a 3D printed 90° elbow, integrated into a flow loop, was developed to evaluate erosion-corrosion of X65 carbon steel along both the inner and outer internal portions of the bend in an aqueous carbon dioxide (CO₂)-saturated environment containing sand particles. Designing representative geometries capable of measuring rates of corrosion, erosion and their synergistic interactions, can be challenging and currently no designs have been reported in literature that effectively integrate the required measuring techniques to determine local degradation rates throughout the component. To elucidate the individual contributions to overall erosion-corrosion degradation rates, gravimetric and electrochemical measurement techniques were used to quantify degradation rates at multiple locations in the flow geometry, with the specimen design also enabling the possibility of completing acoustic emission measurements to detect particle impacts. The design of the elbow is presented and erosion-corrosion tests were conducted to determine the magnitude and individual contributions of erosion, corrosion and erosion-corrosion interactions at a flow velocity of 6 m/s in a CO₂-saturated, pH 4, 60°C, 2 wt.% NaCl solution containing 1000 mg/L of sand particles.

1. Introduction

Erosion-corrosion of pipelines is a significant problem affecting many industries, including oil and gas, and involves electrochemical, mechanical and synergistic processes [1]. The presence of carbon dioxide (CO₂) and the entrainment of sand particles in the

produced slurry results in a highly aggressive wear environment for pipelines, particularly when they are manufactured from carbon steel. Hydrodynamic conditions, which are dictated to a certain extent by the flow geometry, can significantly influence erosion-corrosion degradation rates. The hydrodynamic regime can influence corrosion kinetics through enhancing mass-transfer processes, and the flow field also plays a critical role in influencing the trajectories and velocities of sand particles which impinge onto the internal walls of a system [2, 3]. As a result of this, pipeline components which create significant disturbances in the flow (i.e. abrupt changes in geometry) can be susceptible to high rates of erosion-corrosion degradation [4, 5].

The total erosion-corrosion degradation rate can be broken down into four constituent components, as shown in Equation (1). The total erosion-corrosion material loss (EC_{TML}) consists of a pure erosion (E_0) component, a flow-induced corrosion (C_{FIC}) component and interactions between erosion and corrosion in the form of erosion-enhanced corrosion (ΔC_E) and corrosion-enhanced erosion (ΔE_C) [6]. To fully understand erosion-corrosion and the contributions of the individual mechanisms to total degradation rates, each term in Equation (1) must be quantified.

$$EC_{TML} = C_{FIC} + E_0 + \Delta C_E + \Delta E_C \quad (1)$$

Although several parameters influence the corrosion and erosion mechanisms, the flow regime plays a particularly important role by affecting both mechanisms. It has been widely reported that particle impact angle and particle impact velocity have a significant influence on both erosion rates and the mechanisms of material removal after particle impingement [2, 7-9]. Impact angle is critical in defining the erosion degradation mechanisms, with plastic deformation observed at high impact angles and cutting observed at lower impact angles for ductile materials [9]. The fluid transporting the particles influences both the impact angle and impact velocity, highlighting the significance of flow geometry on erosion mechanisms [2].

Flow is also an influential parameter in the context of pure corrosion of carbon steel in CO₂-saturated conditions when no sand is present [3, 10]. In low pH environments (pH ~4) increased flow velocity accelerates corrosion rates of carbon steel in conditions when protective surface films, such as corrosion inhibitor films or corrosion products, are not present, by increasing the transport of electrochemically active species to and from the corroding metal [3]. In such conditions at low pH, and in the absence of surface

corrosion products, corrosion rates of carbon steel have been shown to vary between different test geometries despite completing tests at the same flow velocities, due to discrepancies in the rates of mass transfer [11]. Therefore, flow geometry has a significant influence on both corrosion and erosion mechanisms and hence erosion-corrosion degradation, making erosion-corrosion experimental evaluation challenging.

Several test geometries have been used for erosion and erosion-corrosion testing, including slurry pot tests and submerged impinging jets (SIJs) [12-29]. SIJs are one of the most commonly used methods for erosion-corrosion testing, being ideal for completing analysis of high velocity flow across a range of temperatures and brine chemistries in sand-laden conditions. SIJs are very effective for investigating erosion-corrosion but hydrodynamic conditions and sand impingement characteristics can vary dramatically over the surface of a test specimen, making quantifying degradation rates accurately for a particular set of operating conditions challenging [28, 30]. However, this can be advantageous as the SIJ can be used to replicate a wide range of field conditions in a single experiment. The SIJ has been used to relate CFD predicted impact angles to erosion degradation, enabling erosion rate maps to be constructed for a wide range of impact conditions through analysis of wear depth across a carbon steel specimen after SIJ erosion tests [18]. The SIJ has also been used to analyse mechanisms of erosion-corrosion degradation of X65 carbon steel after particle impingement at different impact angles on the surface [28]. However, regions of the specimens used in the SIJ are subjected to flow-induced corrosion conditions that are not always representative of those in pipe flow geometries [10, 31]. Therefore, achieving both erosion and flow-induced corrosion conditions on a sample surface in the SIJ that are equivalent to the application of interest may not always be possible. It has been shown that the contribution of erosion mechanisms and corrosion mechanisms can significantly influence erosion-corrosion interactions of carbon steel, therefore, accurately recreating the contributions of corrosion and erosion expected in field conditions is essential for representative erosion-corrosion investigations [28].

Direct impingement test cells, contained within flow loops, have also been used to study mechanisms of erosion-corrosion in various experimental conditions relevant to the oil and gas industry [32-36]. The test cell was used to investigate erosion-corrosion multiphase flow conditions [32], to assess corrosion inhibitor performance in sand-

containing environments [33], to assess the significance of sand particle impingement on the integrity of corrosion products [34, 35] and to assess the influence of high sodium chloride (NaCl) concentrations on erosion-corrosion of carbon steel [36]. Samples were positioned opposite to a nozzle, similarly to SIJ tests, but the apparatus was capable of being used for much higher flow velocities, up to 60 m/s [33]. Similar challenges, as were highlighted for the SIJ, are likely to also be a factor when using this test cell, as the exact appropriate combination of corrosion and erosion conditions may not always be achievable to replicate the field conditions of interest.

The use of a laboratory-based pipe flow geometry is, therefore, required for evaluating erosion-corrosion rates anticipated in pipe flow when alternative geometries do not accurately represent flow and particle impingement conditions. Although there has been some research conducted to investigate erosion-corrosion in pipe flow geometries [37-42], the complexity of erosion-corrosion studies have meant that existing designs have not integrated multiple measurement techniques, preventing the determination of all terms identified in Equation (1) at multiple locations in the geometry, whilst ensuring no disturbance of the flow as result of using multiple, isolated test specimens.

In reference to previous studies, Shadley et al. [37, 38] inserted a 90° carbon steel elbow specimen into a flow loop, capable of being used for measuring mass loss and thickness loss after being subject to erosion-corrosion experiments. This geometry was successfully used to measure degradation rates and identify regions of interest in the elbow experiencing high degradation rates. However, the use of a single elbow specimen prevented isolated electrochemical measurements from being completed that could be used to determine local individual contributions of all terms in Equation (1). The elbow designed by Zeng et al. [39, 40] integrated multiple, isolated carbon steel specimens, enabling electrochemical and gravimetric measurements to be completed at multiple locations in the elbow. However, the accuracy of the measurements could have potentially been limited by flow disturbances in the component, caused by the method used to position and mount the specimens in the elbow body. Finally, Rincon et al. [41, 42] completed studies of erosion-corrosion degradation in multiphase, sand-laden flows, by flush-mounting a measurement probe into both a plugged tee and elbow, integrated into a flow loop. This was very effective for studying degradation mechanisms and determining precise local erosion-corrosion rates. However, the integration of multiple

sensing elements within a flow component could provide even greater insight into degradation rates and mechanisms.

In this study, the authors present the development of a 3D printed 90° degree elbow [43], used for erosion-corrosion experimental studies, capable of utilising gravimetric, electrochemical and acoustic emission measurement techniques at multiple locations within the geometry. Curved specimen design enabled flush-mounting of specimens into the geometry, ensuring a realistic pipe flow regime and enabling local degradation rates to be determined throughout the geometry. The methodology for developing the geometry is presented, demonstrating the potential to create other similar rapid prototyped geometries for improved studies of erosion-corrosion in different applications of interest.

2. Elbow Design

2.1. Design Overview

The elbow was designed to improve the test methodology for erosion-corrosion analysis in geometries representative of field pipe flow conditions [43]. The field conditions and geometry of interest, which this study was based on, could not be represented accurately using an SIJ or through the mapping of wear rates (as in other studies involving pure erosion [18]), as the desired combination of mass transfer coefficients and particle impingement characteristics could not be achieved. This meant that a pipe flow design was more appropriate to model the combined degradation process. The aim of this design was to be able to create a pipe flow component that could meet the following design criteria:

- i. Developed using a cost-effective, rapid prototyping manufacturing technique;
- ii. Manufactured from a corrosion resistant material that would not experience significant erosion degradation to produce a robust component that could be used for long-term testing in high velocity erosion-corrosion conditions;
- iii. Developed to be integrated into a flow loop;
- iv. Capable of utilising different measurement techniques (mass loss, electrochemical and acoustic emission techniques) required to determine degradation rates and mechanisms of material loss for each of the terms in Equation (1);
- v. Fully sealed to prevent leakage of fluid and ingress of oxygen (O_2).

The fully assembled elbow design is shown in Figure 1. The body of the elbow consisted of an outer radius (1) and an inner radius (2), with the elbow being split to ensure that specimens could be positioned and adequately flush mounted prior to starting experiments. Twelve metal specimens (3) were fitted into the elbow at specific angles with an equal number of specimens located on both the inner and outer radius of the elbow, enabling erosion-corrosion degradation rates and their individual corrosion and erosion components to be determined throughout the elbow. Specimen holders (4) were used to fix the specimens in the elbow body and to provide sealing pressure to the O-rings positioned around the specimens used to prevent leakage of fluid. Grooves (5) were designed into the elbow body so that flow loop piping could be fitted into the elbow body using O-rings, fixed together using a series of bolts around the elbow body used to fasten the inner and outer radius together (6). The grooves in the elbow allowed flow loop piping to be securely fitted and flush-mounted in the elbow, making it convenient and easy to fix the elbow into the pipework, ensuring no O₂ ingress during experiments. Two O-rings were fitted around each of the inlet and outlet flow loop pipes that could be positioned in the elbow body, before the inner radius and outer radius were fastened together. O-ring cord (7) was positioned in grooves on both sides of the internal flow diameter to prevent leakage through the elbow body halves.

An internal diameter (D_p) of 25.4 mm (1 inch) was used to maintain the same flow diameter as the inner diameter of the flow loop pipes into which the elbow assembly was fitted. The elbow radius (R) was equal to five times the internal diameter of the elbow ($R/D_p = 5$). This R/D_p ratio was chosen to be representative of typical elbow geometries used in the field. McLaury et al. [44] showed that erosion rates decreased as the R/D_p ratio was increased. However, significant erosion was still expected in an elbow with an R/D_p ratio of 5 based on their results. Twelve specimens were fitted into the elbow at angles of 0°, 15°, 35°, 55°, 75° and 90°, with a specimen located on both the inner and outer radius at each of these angles. This quantity of specimens was chosen so that a sufficient number of regions could be analysed in the elbow, within the geometrical limits of the design, whilst also ensuring that specimens were of a sufficiently large diameter in order to ensure satisfactory quality and accuracy of mass loss measurements collected.

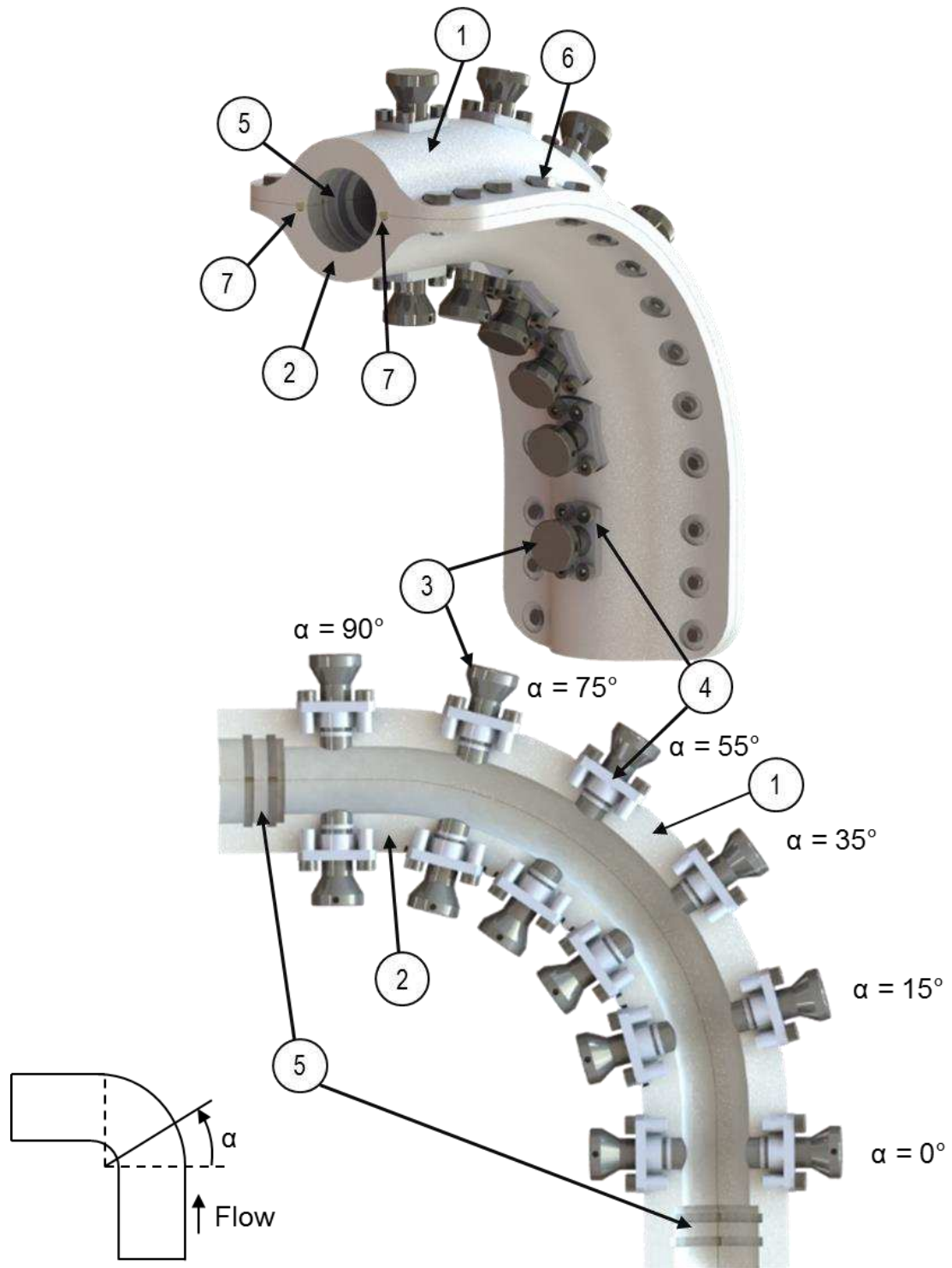


Figure 1: Fully assembled elbow design consisting of (1) body outer radius, (2) body inner radius, (3) test specimens x 12, (4) specimen holders x 12, (5) flow inlet and outlet grooves, (6) bolts x 28 to faster inner and outer radius together and (7) O-ring cord x 2, where α is the angle in the elbow used to identify specimen locations [43]

2.2.Test Specimen Design

The specimen design used in the elbow is shown in Figure 2. Several factors influenced the design of the specimens. The specimen surface exposed to the flow required curvature with the same radius as that of the flow channel in the elbow, as a flat specimen surface would have resulted in protrusion into the flow field, disrupting the fluid hydrodynamics, resulting in conditions that were unrealistic and unrepresentative of pipe flow conditions. Specimens could be fitted and removed from the elbow to complete mass loss measurements to determine degradation rates. The procedure for inserting specimens and removing specimens from the elbow body is shown in Figure 3. Flush-mounting was confirmed prior to fastening the two halves the elbow together. To prevent crevice corrosion, a lacquer coating was applied around the edges of the specimens.

Based on experience, an exposed surface area of $\sim 1 \text{ cm}^2$ to the flow field was required so that sufficient mass loss would be measured without measurement error posing a significant problem. It was also equally important to ensure that the surface area was not so large that local erosion-corrosion conditions, in terms of impingement angles, impingement velocities and flow parameters, varied significantly over the specimen surface. A specimen diameter of 12 mm was therefore used, resulting in a surface area of 1.16 cm^2 being exposed to the flow for each test specimen. Due to the size of the specimens, a maximum of six could be fitted into each radius of the elbow (making twelve specimens in total).

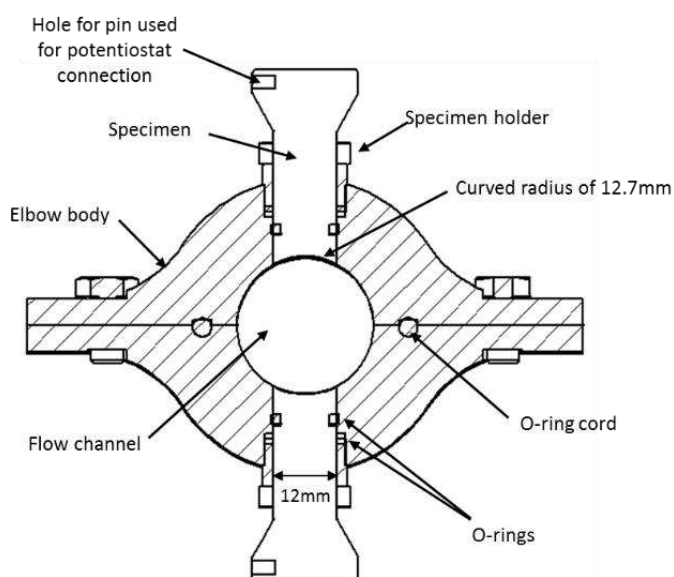
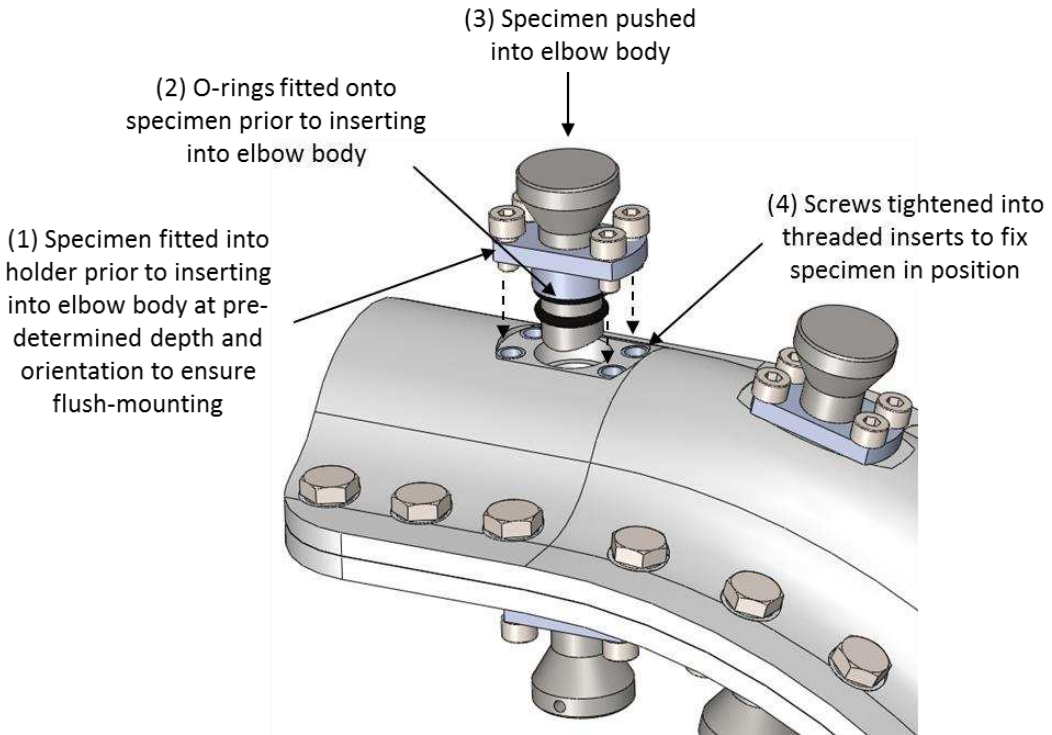


Figure 2: Test specimens used in the elbow with a curved radius, indicating how the specimens were mounted and fixed into the body of the elbow



**Figure 3: Procedure for inserting and securing specimens in the elbow body.
Removal of specimens was completed in reverse order**

2.3.Measurement Techniques

Multiple measurement techniques were required to elucidate the corrosion and erosion mechanisms in Equation (1). Mass loss measurements can be used to determine reliable corrosion rates in steady-state, non-film forming conditions. For mass loss measurements, specimens were removed from the elbow after tests to determine degradation from mechanical and electrochemical mechanisms. Electrochemical measurement techniques could also be completed by using the specimens as working electrodes as part of a three electrode cell, along with a reference electrode and counter electrode fitted into the flow loop, shown later. Carbon steel pins were inserted into the drilled holes in the specimen, to enable convenient connection to a computer controlled potentiostat.

The specimens were designed with a tapered shape for the purpose of acoustic emission monitoring using a sensor which required a diameter larger than 12 mm (the specimen diameter exposed to the flow internally in the elbow) for the detection of acoustic energy from particle impacts. Acoustic emission measurements were completed successfully by Ukpai et al. [45, 46] to detect the acoustic energy as a result of sand particle impacts on

the surface of carbon steel specimens in SIJ tests. Acoustic emission results are not reported in this study and are being completed as part of ongoing work using the geometry.

2.4.Manufacturing

The elbow body and specimen holders were 3D printed using a Stratasys Objet 1000 Plus 3D printer, with a printing time of approximately 15 h. Due to the aggressive nature of the testing environment, elbow components could easily be replaced if they suffered any wear from excessive use, however, no indication of degradation of the 3D printed elbow was observed at the end of the series of tests performed in this study, demonstrating the durability of the components. The outer radius, inner radius and specimen holders were 3D printed using acrylonitrile butadiene styrene (ABS) material. ABS provides adequate strength and chemical resistance properties to cope with the demands of erosion-corrosion tests [47]. This also enabled electrochemical measurements to be completed by isolating specimens from the elbow body.

2.5.Integration into a Flow Loop

A diagram showing how the elbow was integrated into the flow loop is shown in Figure 4. The flow loop is able to contain a sand-laden solution which could be pumped through the elbow continuously. The flow loop system consisted of a variable frequency centrifugal pump (Lowara) used to recirculate the solution and a 50 L reservoir to accommodate the brine solution and sand particles. The pipework of the flow loop was easily modified and components could be quickly removed or replaced to change the geometry of the flow to the required conditions.

Sections of pipe from the flow loop were removed so that the elbow could be fixed into place securely. The pipework in the flow loop consisted of 25.4 mm internal diameter and 32 mm outer diameter chlorinated polyvinyl chloride (PVC-C) pipes, enabling use of the flow loop in temperatures up to 80°C. Sections of pipe were connected using PVC-C unions and fittings to change the geometry of the flow, such as elbows. PVC-C unions and fittings were cemented together to provide a seal and to fix components in position. Two short sections of PVC-C pipe were cemented into separate unions and inserted into the inlet and outlet of the elbow so that it could be fastened into the flow loop pipework, as

shown in Figure 4. The elbow was positioned at a distance of approximately 40 internal diameters downstream of the pump so that the flow could develop after exiting the pump and approximately 10 internal diameters of straight pipe was fitted after the elbow to minimise disruption to the flow in the elbow. A minimum of 10 internal diameters is required prior to inlet to allow the flow to fully develop in turbulent pipe flow [48]. A stainless steel cooling tube was fitted into the flow loop to maintain solution temperature during testing as heat from the pump was prone to raising solution temperature. The stainless steel tubing had similar dimensions to the titanium heating element which was also present in the reservoir and was fitted into the reservoir lid. A redox silver/silver chloride (Ag/AgCl) reference electrode incorporating a platinum (Pt) counter electrode was fitted downstream of the elbow, so the flow was not disturbed within the elbow itself.

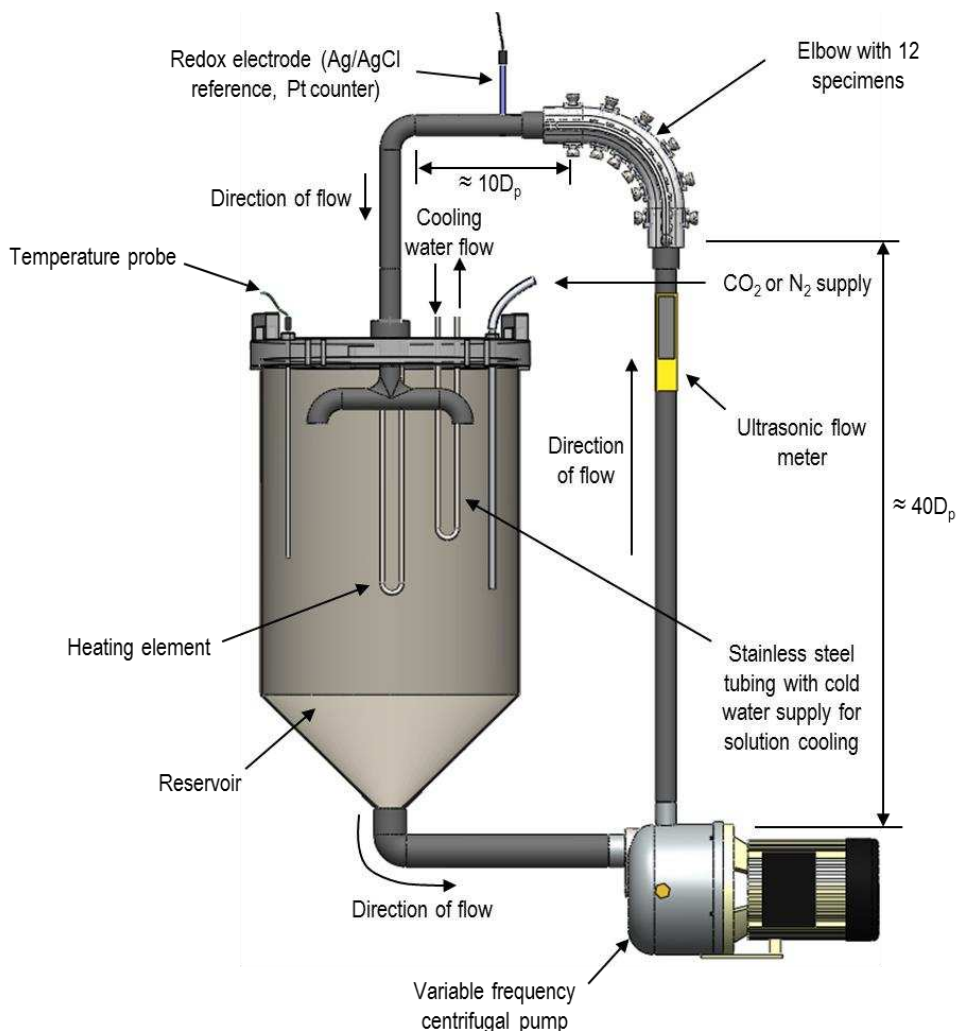
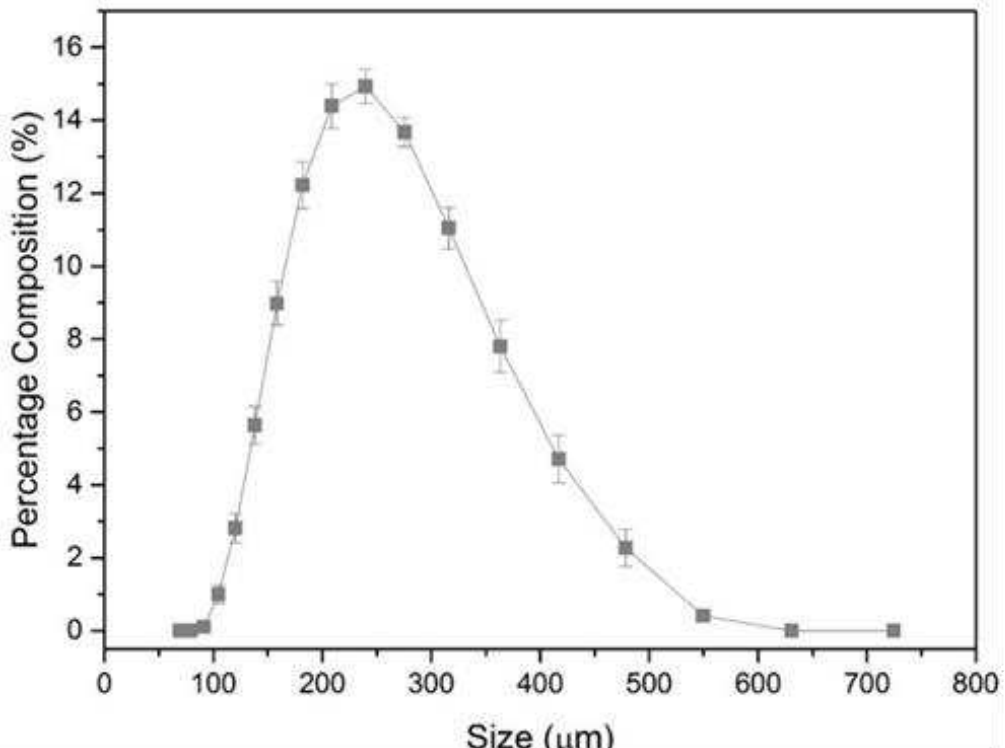


Figure 4: Diagram of the elbow integrated in a flow loop, where D_p is the internal pipe diameter

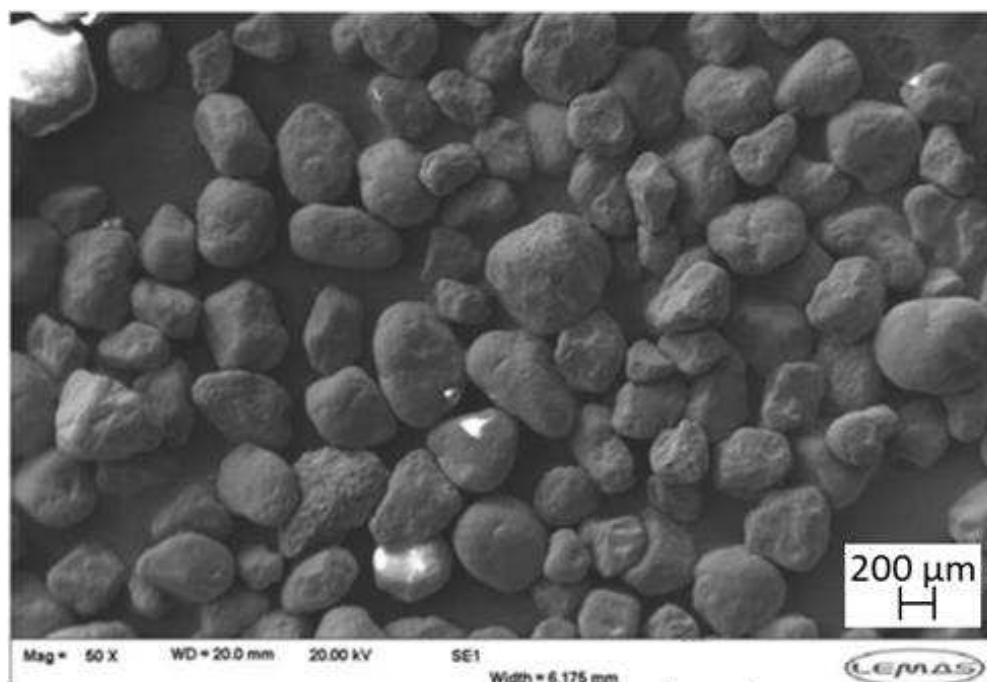
3. Experimental Methodology

Flow-induced corrosion (no sand), erosion (N_2 -saturated with no corrosion) and erosion-corrosion tests were completed using the elbow to elucidate the components of degradation referred to in Equation (1) and demonstrate the performance of the elbow. For flow-induced corrosion and erosion-corrosion tests, CO_2 was bubbled into the 50 L deionised water solution containing 2 wt.% NaCl in the flow loop reservoir for a minimum period of 12 h to reduce dissolved O_2 in the solution to less than 50 ppb (confirmed previously through the application of a colorimetric technique). After saturation, the solution pH was measured to ensure it was stable at pH 4. N_2 was bubbled into 50 L deionised water for pure erosion tests at pH \sim 7, to produce a minimally corrosive environment to measure pure erosion degradation. Gas was bubbled into the solution in atmospheric conditions, resulting in a partial pressure of approximately 0.8 bar. The solution was continuously recirculated during the sparging period for all tests, before the elbow was fitted into the system to ensure that conditions were consistent throughout the entire solution and that as much O_2 was removed from the system as possible.

The grade of sand particles used was HST60, with an average particle diameter of 250 μm and size distribution as shown in Figure 5. Sand particles were added to the solution reservoir in a concentration of 1000 mg/L for erosion and erosion-corrosion tests prior to starting the test. An SEM image of the sand particles is also shown in Figure 5, showing that sand particles were not perfectly spherical and had various irregular shapes. To determine the sand concentration flowing through the elbow, comparison of the actual sand concentration flowing through the elbow prior to completing experiments (measured by filtering and drying sand particles from a known volume of fluid extracted from the pipe flow at a flow velocity of 6 m/s), was compared to the known sand concentration added to the 50 L flow loop reservoir. At a flow velocity of 6 m/s, the actual sand concentration flowing through the elbow was equal to the sand concentration added to the reservoir, confirming sand was not settling in the flow loop.



(a)



(b)

Figure 5: HST60 sand particles used in erosion and erosion-corrosion SIJ tests showing (a) size distribution of the particles and (b) SEM image of sand particles [27]

The deionised water solution was recirculated using the variable frequency pump at a flow velocity of 6 m/s, measured at the inlet of the elbow using an ultrasonic flow meter (Micronics), positioned on the PVC-C pipes as shown in Figure 4. Flow velocities in excess of 6 m/s could be tested, but these conditions were chosen to replicate the field. Tests were completed in a solution at a temperature of 60°C, set and maintained using a temperature controller and temperature probe. As previously stated, at high pump frequencies, required for 6 m/s flow velocities, the solution temperature increased during tests. Therefore, the solution was cooled in the reservoir using a stainless steel tube connected to a cold water supply. The flow rate of the cooling water was maintained during tests to ensure a constant solution temperature was achieved throughout the test. The temperature of the solution could be heated to the desired temperature using the heating element and the cooling system could maintain the temperature throughout the test.

For the tests completed in this work, X65 carbon steel, a common pipeline grade carbon steel, was used as a test specimen, with the composition as shown in Table 1. However, any metal specimen could be fitted into the elbow if manufactured to the appropriate dimensions. The specimens were ground by hand prior to testing using 320, 600, 800 and 1200 grit silicon carbide grinding paper sequentially to achieve a consistent surface finish across all specimens prior to testing. Mass loss and electrochemistry techniques were used to determine degradation rates of the specimens during tests. After grinding by hand, specimens were degreased with acetone, rinsed with distilled water and dried prior to measuring the mass of the specimen using a mass balance with a precision of ± 0.01 mg. The mass of each specimen was measured prior to starting tests and after completing tests to determine the mass loss. O-rings and specimen holders were removed from the specimens prior to completing mass loss measurements. Experiments ran for 8 h so that sufficient mass loss could be measured before degradation of sand particles became significant, potentially influencing erosion conditions during the test.

Table 1: X65 carbon steel composition (wt.%)

C	Mn	Ni	Nb	Mo	Si	V	P	S	Fe
0.15	1.422	0.09	0.054	0.17	0.22	0.06	0.025	0.002	97.81

To determine each of the contributing components to total degradation in Equation (1), mass loss measurements were completed. Electrochemical measurements were completed to confirm that corrosion rates were constant throughout the 8 h test period, but were not relied upon for accurate corrosion rate prediction. X65 specimens were used as working electrodes and connected to an ACM Gill 12-channel computer controlled potentiostat. X65 specimens were used as working electrodes with a Pt counter electrode and Ag/AgCl reference electrode used to form a three electrode cell. Linear polarisation resistance (LPR) measurements were conducted during tests to determine the corrosion rates of the specimens in a scan range from -15 mV to +15 mV relative to open circuit potential at a scan rate of 0.25 mV/s. LPR measurements were completed sequentially. Therefore, a single measurement was completed on each specimen separately, starting at the inlet specimens and ending at the outlet specimens, alternating between the specimens on the inner and outer radius at each angle until all measurements were completed. The same measurements were completed in cycles, with one cycle of measurements requiring approximately 25 - 30 minutes to complete. Scan cycles were completed continuously throughout the test duration.

4. Results & Discussion

4.1. Flow-Induced Corrosion

The comparison of corrosion rates on the inner and outer radius determined from mass loss techniques in flow-induced corrosion tests are shown in Figure 6. Similar corrosion rates were measured on the inner and outer radius of the elbow, with slightly higher corrosion rates measured on the outer radius of the elbow at the 35°, 55° and 75° angle specimens. Corrosion rates on both the inner and outer radius increased at the exit of the elbow on the 90° specimens. Zeng et al. [39] reported similar increased corrosion rates at the outlet in experiments completed in an elbow at a flow velocity of 4 m/s in a 60°C, CO₂-saturated solution, but a slightly greater difference in corrosion rates on the inner and outer radius was observed than shown in Figure 6. Two repeat measurements were completed with the average measurement of the results reported.

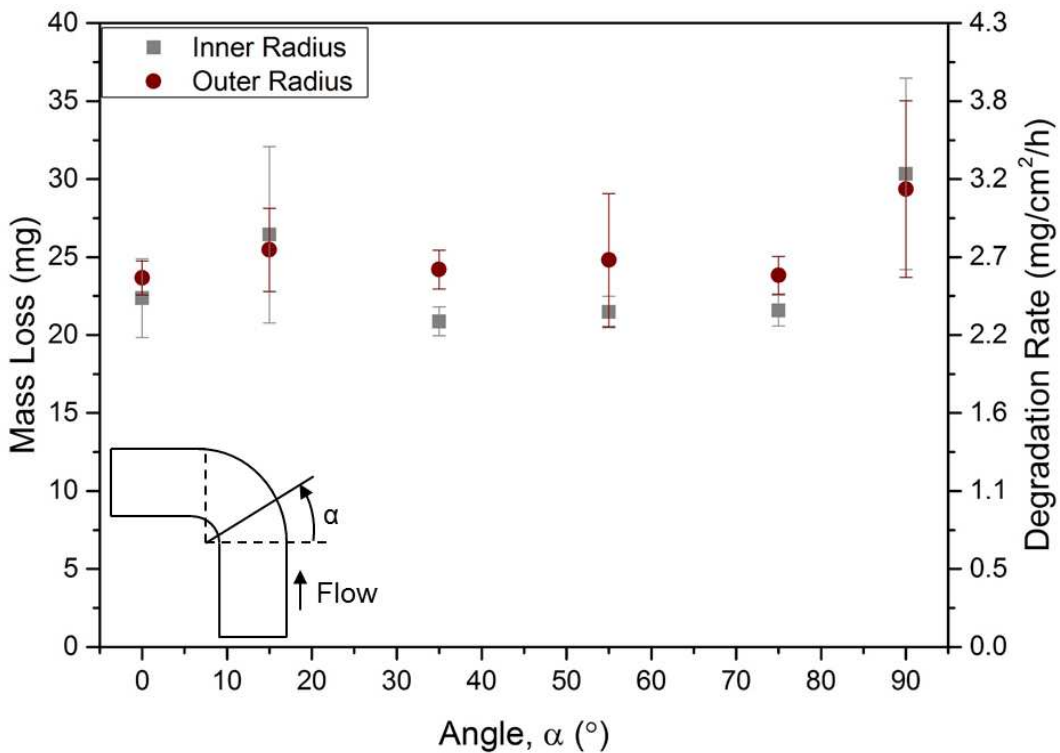


Figure 6: Comparison of mass loss measured corrosion rates of X65 carbon steel specimens on the inner and outer radius of an elbow in flow-induced corrosion tests at a flow velocity of 6 m/s in a 2 wt.% NaCl, pH 4, CO₂-saturated solution at 60°C, where α refers to the position of the specimen in the elbow

To demonstrate that corrosion rates remained constant during the 8 h test period and that mass loss measurements were representative of corrosion rates throughout a test, polarisation resistances ($1/R_p$) from LPR measurements are shown over a period of 8 h on the inner and outer radius in Figure 7 and Figure 8. The average from two repeat measurements is shown. In steady-state conditions with no variation in Tafel constants, corrosion rates are proportional to $1/R_p$. However, correction of R_p to determine corrosion rates by compensating for solution resistance and using Tafel constants can cause propagation of error that can cause some variation in corrosion rates. Calculation of interactions using Equation (1) relies on accurate corrosion measurements, therefore mass loss was most reliable. A constant value of R_p was observed shortly after starting the test on all of the specimens on the inner and outer radius, showing that corrosion rates did not vary during a test and that mass loss measurements were representative of the degradation rates measured during a test. Some variation was observed at the start of tests, potentially as the system reached equilibrium conditions after the pump was switched on at the start of the test.

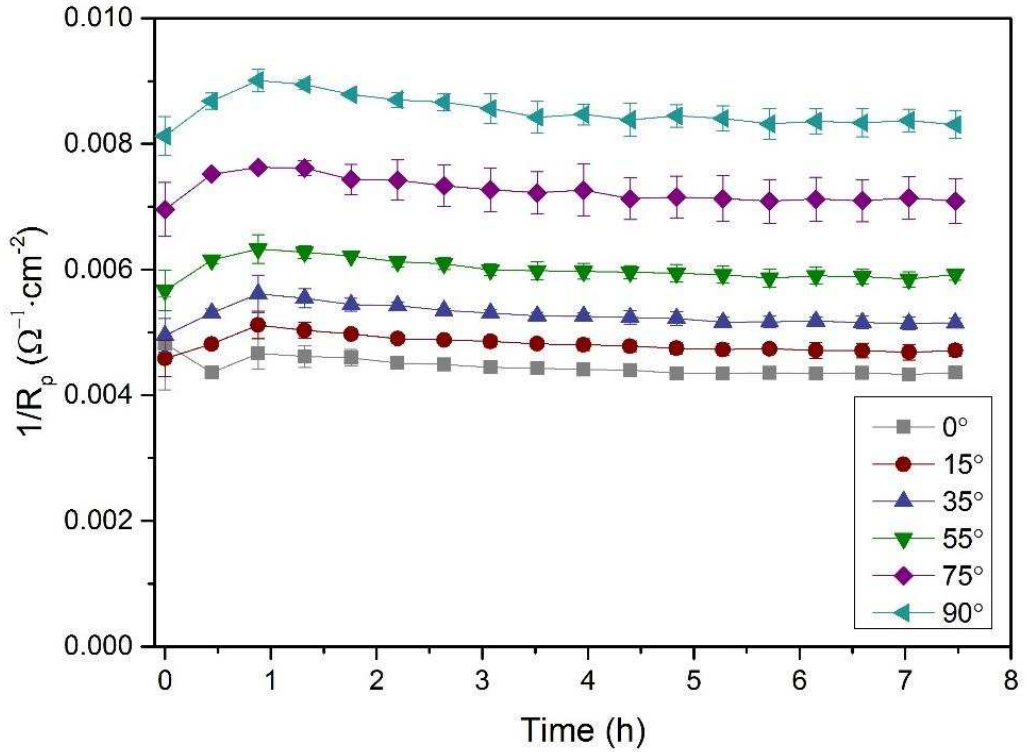


Figure 7: Comparison of polarisation resistance from LPR measurements on the inner radius of an elbow in flow-induced corrosion tests at a flow velocity of 6 m/s in a 2 wt.% NaCl, CO₂-saturated solution at 60°C

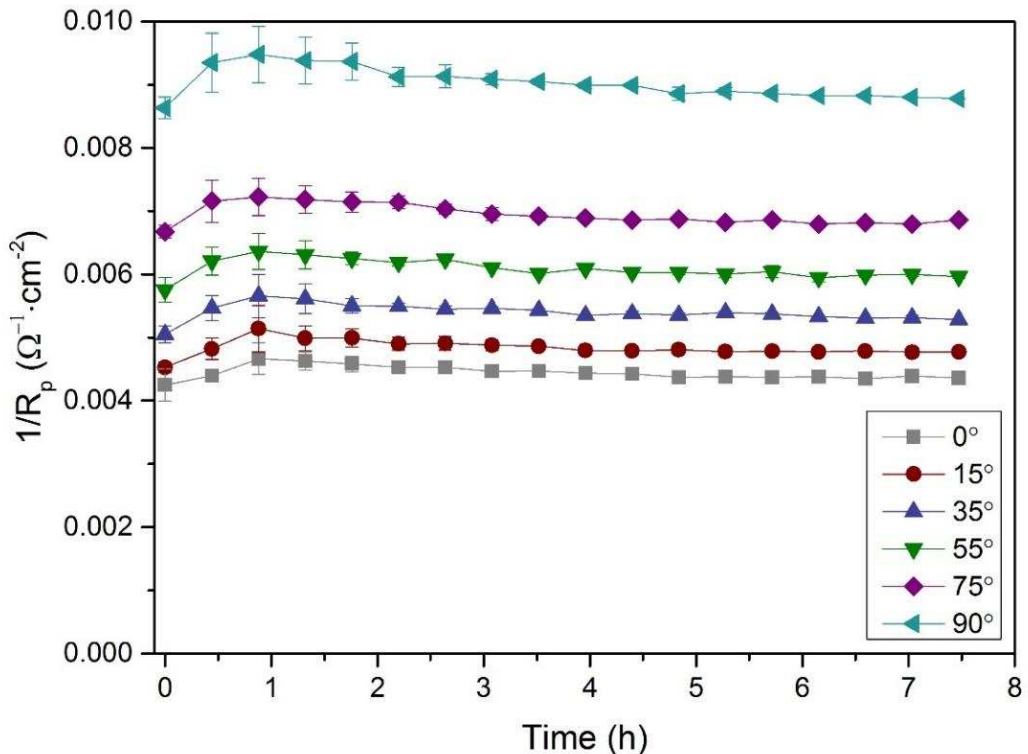


Figure 8: Comparison of polarisation resistance from LPR measurements on the outer radius of an elbow in flow-induced corrosion tests at a flow velocity of 6 m/s in a 2 wt.% NaCl, CO₂-saturated solution at 60°C

4.2.Erosion-Corrosion

The comparison of degradation rates of X65 measured from flow-induced corrosion tests without sand, erosion tests in N₂-saturated sand-laden conditions and erosion-corrosion tests in sand-laden CO₂ conditions on the inner radius and outer radius of the elbow are shown in Figure 9 and Figure 10. The angle, α , reported refers to the position in the elbow where the specimens are located and not the particle impact angle. No erosion was measured on the inner radius of the elbow, with erosion-corrosion rates and flow-induced corrosion rates being very similar. A slight increase in degradation was measured on the outer radius of the elbow in erosion-corrosion conditions, with erosion from particle impingement making a small contribution to total erosion-corrosion degradation. CFD predictions of erosion in elbows have shown that the majority of particle impacts occur on the outer radius of the elbow [49]. The most significant increase in degradation rate in erosion-corrosion conditions was observed at the 75° specimen.

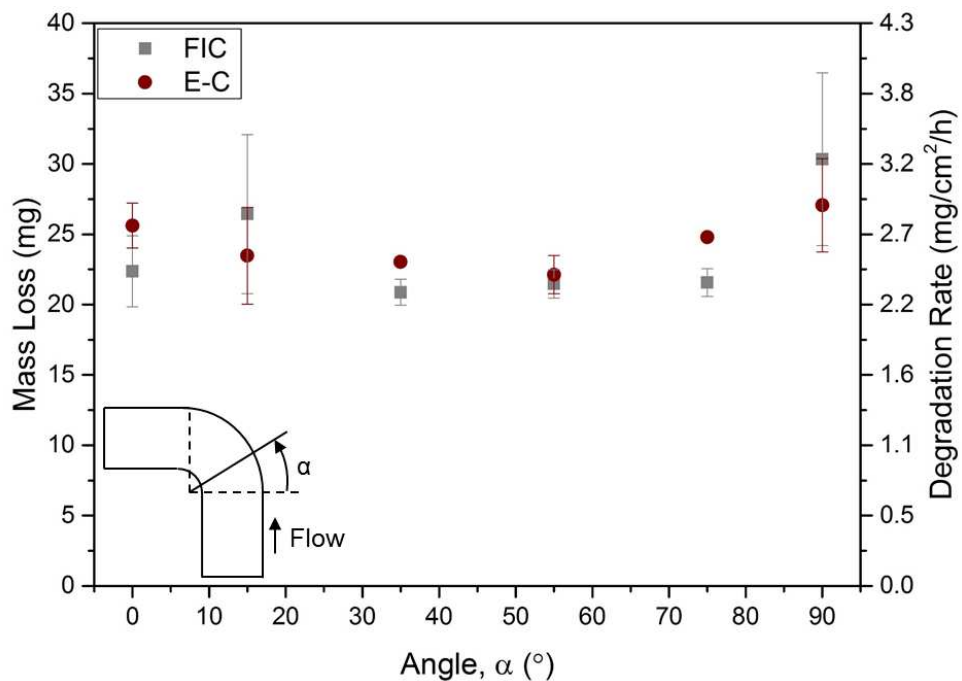


Figure 9: Degradation rate from mass loss of X65 carbon steel specimens on the inner radius of an elbow in flow-induced corrosion (FIC) tests at a flow velocity of 6 m/s in a 2 wt.% NaCl, CO₂-saturated solution at 60°C and erosion-corrosion (E-C) tests containing 1000 mg/L of sand, where α refers to the position of the specimen in the elbow

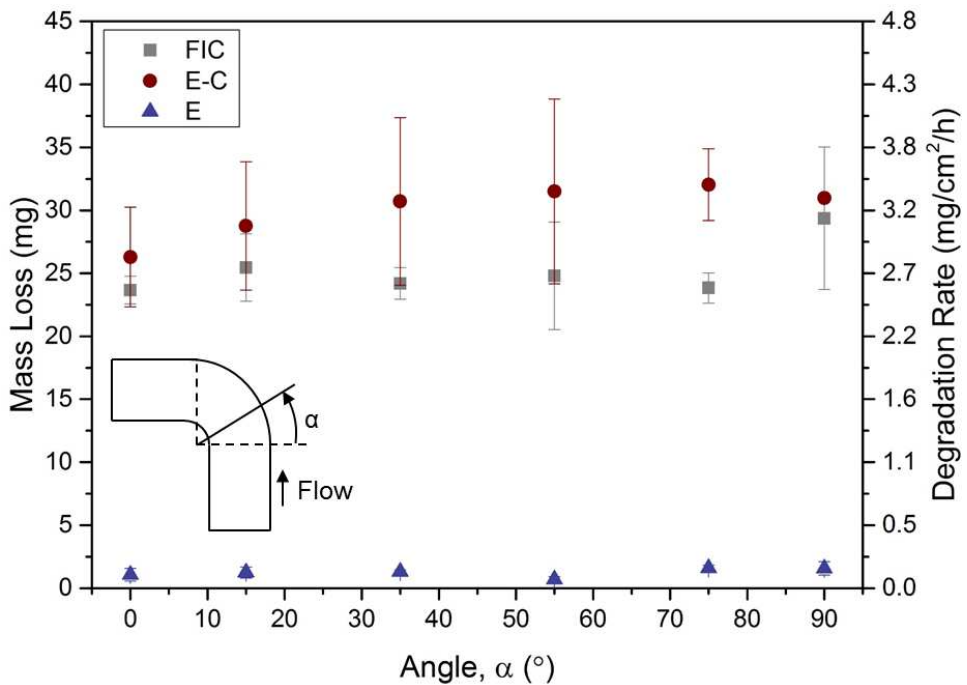


Figure 10: Degradation rate from mass loss of X65 carbon steel specimens on the outer radius of an elbow in flow-induced corrosion (FIC) tests at a flow velocity of 6 m/s in a 2 wt.% NaCl, CO₂-saturated solution at 60°C, pure erosion (E) tests and erosion-corrosion (E-C) tests containing 1000 mg/L of sand, where α refers to the position of the specimen in the elbow

The contribution of the individual mechanisms to total erosion-corrosion degradation is shown in Figure 11 for each of the six specimens on the outer radius, where 'EC_{TML}' represents the total erosion-corrosion material loss measured from mass loss tests. 'C_{FIC}' represents the total flow-induced corrosion rate measured from mass loss tests. 'E₀' is the pure erosion rate measured from erosion tests in N₂-saturated conditions. ' $\Delta C_E + \Delta C_C$ ' represents the contributions of erosion-enhanced corrosion and corrosion-enhanced erosion. The contribution of erosion-enhanced corrosion and corrosion-enhanced erosion was determined by rearranging Equation (1) and deducting the experimentally measured pure corrosion rate and pure erosion rate from the total erosion-corrosion degradation rate. Error in the measurements of erosion-corrosion, erosion and corrosion rates propagated in the calculation of the interaction term, explaining the large error bars shown in Figure 11.

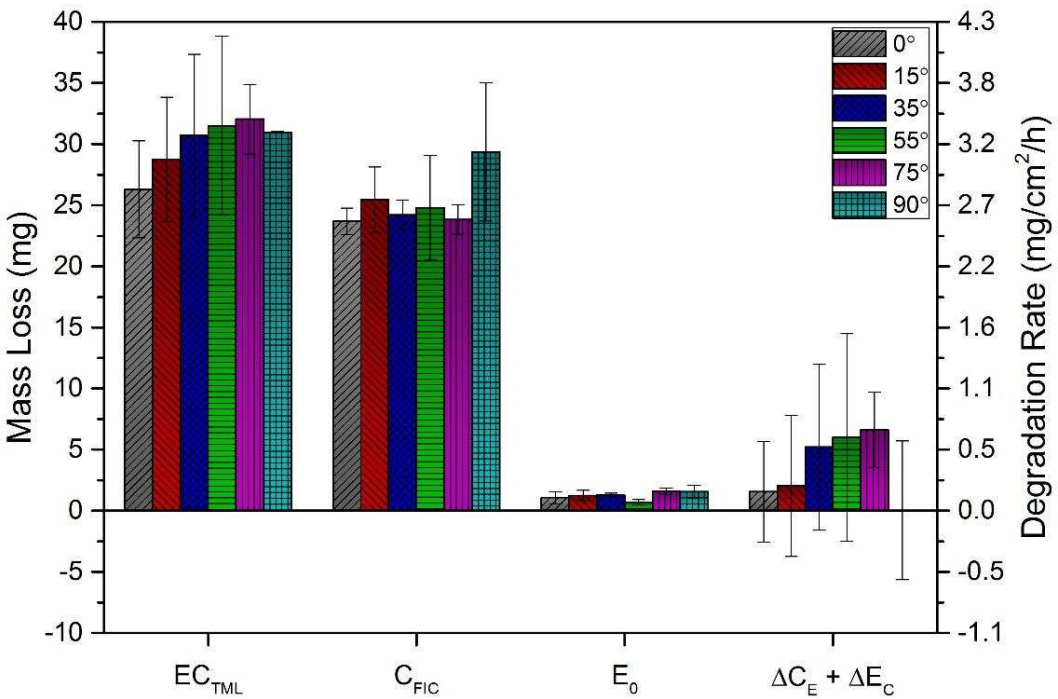


Figure 11: Contribution of corrosion (C_{FIC}), erosion (E_0) and interactions ($\Delta C_E + \Delta E_C$) to total erosion-corrosion (EC_{TML}) degradation on the outer radius of the elbow at a flow velocity of 6 m/s in a 60°C solution containing 1000 mg/L of sand

The contribution of the interactions to total erosion-corrosion degradation was small, but errors did account for a significant proportion of the calculations, as is common in erosion-corrosion research [21, 26]. Due to the significance of error in the calculation of corrosion-enhanced erosion and the required use of electrochemical techniques to determine erosion-enhanced corrosion rates, separating corrosion-enhanced erosion and erosion-enhanced corrosion could not be completed without leading to large ambiguity. SJJ erosion-corrosion experiments conducted using X65 carbon steel in similar conditions (60°C and 2 wt.% NaCl solution containing 1000 mg/L of 250 μm diameter HST60 sand particles) completed at a higher flow velocity of 20 m/s have shown error is less significant in results due to the higher contribution of interactions to overall degradation rate, with corrosion-enhanced erosion being considerably greater than erosion-enhanced corrosion rates [28].

Pure corrosion accounted for approximately 75-90% of total degradation at all specimens. The synergistic component of wear was not as significant in the elbow test results in this paper compared to the results observed by Hu and Neville [21] and Malka et al. [4]. As explained, it could not be determined if the interactions were from corrosion-enhanced erosion or erosion-enhanced corrosion, but combined effects and pure erosion

contributions accounted for a much smaller proportion of degradation on all specimens in this study. Malka et al. [4] reported that corrosion-enhanced erosion was a significant contributing factor and Hu and Neville [21] reported that it was most significant proportion of overall degradation in erosion-corrosion tests at a flow velocity of 20 m/s. It was expected that erosion would not be as significant in the elbow due to the lower flow velocity. However, Malka et al. [4] observed pure erosion rates greater than the erosion rates measured in elbow tests in this paper, despite tests being run at a lower temperature and a lower flow velocity of 2 m/s, which would typically result in lower erosion rates. A much lower quantity of sand was added to the solution in elbow tests, but it was likely that flow geometry was significant on the measured erosion rates in the two studies.

Future work aims to integrate acoustic emission measurements into the analysis of erosion and erosion-corrosion in the elbow to provide further insight into the mechanisms of degradation as a result of particle impingements at multiple locations in an elbow. Ukpai et al. [45, 46] completed acoustic emission studies of erosion in a submerged impinging jet to determine how parameters such as particle impact energy and impact frequency, related to erosion degradation rates and mechanisms on carbon steel surfaces after particle impingement. Conducting acoustic emission studies using the elbow would significantly enhance the understanding of erosion mechanisms and erosion rates, as parameters, such as impact energy and impact frequency, for example, could be compared at different positions in the elbow.

Pure corrosion rates were high in the elbow in the high temperature and low pH conditions tested. These conditions would have contributed to higher pure corrosion rates in the elbow compared with the corrosion rates measured by Malka et al. [4]. However, changes in geometry did have a significant effect on the corrosion rate, which increased at the specimens towards the exit of the elbow, demonstrating how degradation rates can change within a pipe component. When comparing the results in this paper with the results obtained by Malka et al. [4] and Hu and Neville [21], it was clear that several factors, including test geometry influenced results. Therefore, it is essential that the conditions in the specific erosion-corrosion application being analysed are fully understood when completing laboratory-based erosion-corrosion tests that attempt to replicate conditions, which can be recreated through geometry design, and

that individual erosion, corrosion and erosion-corrosion interaction degradation mechanisms can be investigated.

5. Conclusions

The newly-developed elbow geometry, with multiple integrated measurement techniques, was successfully used for erosion-corrosion evaluation, demonstrating the viability of the design for robust erosion-corrosion tests to determine the contribution of corrosion, erosion and interactions to total erosion-corrosion degradation of X65 carbon steel in a pipe flow environment by utilising multiple measurement techniques. The following conclusions were reached:

- Corrosion rates in flow-induced corrosion tests at 6 m/s in a pH 4 solution saturated with CO₂ at a temperature of 60°C were slightly higher on the outer radius and increased on both the inner radius and outer radius towards the outlet of the elbow.
- Erosion tests at 6 m/s and temperature of 60°C were conducted using the elbow and showed that no erosion was present on the inner radius of the elbow and erosion rates were similar at all specimens on the outer radius.
- An increase in degradation rate on the outer radius of the elbow compared to flow-induced corrosion conditions was observed in erosion-corrosion conditions, with the most significant increase on the outer radius at the specimen located at 75° from the inlet.
- Interactions between erosion and corrosion were observed but could not be quantified individually due to the small magnitude of the interactions.
- Variations in the contributions of corrosion, erosion and interactions to overall material degradation were measured compared to results in literature, highlighting the significance flow geometry can have on erosion-corrosion degradation rates and the individual parameters that contribute to total degradation.

Acknowledgements

The authors would like to thank EPSRC and Shell UK for the funding of this research and Graham Brown in the School of Mechanical Engineering at the University of Leeds for assisting in the design and manufacture of the elbow component.

References

1. Burson-Thomas, C.B. and Wood, R.J., *Developments in Erosion–Corrosion Over the Past 10 Years*. Journal of Bio-and Triboro-Corrosion, 2017. **3**(2): p. 14.
2. Humphrey, J.A.C., *Fundamentals of fluid motion in erosion by solid particle impact*. International Journal of Heat and Fluid Flow, 1990. **11**(3): p. 170-195.
3. Nešić, S., *Key issues related to modelling of internal corrosion of oil and gas pipelines – A review*. Corrosion Science, 2007. **49**(12): p. 4308-4338.
4. Malka, R., Nešić, S., and Gulino, D.A., *Erosion–corrosion and synergistic effects in disturbed liquid-particle flow*. Wear, 2007. **262**(7–8): p. 791-799.
5. Nešić, S. and Postlethwaite, J., *Hydrodynamics of disturbed flow and erosion–corrosion. Part II - Two-phase flow study*. The Canadian Journal of Chemical Engineering, 1991. **69**(3): p. 704-710.
6. Madsen, B.W., *Measurement of erosion-corrosion synergism with a slurry wear test apparatus*. Wear, 1988. **123**(2): p. 127-142.
7. Finnie, I., *Some reflections on the past and future of erosion*. Wear, 1995. **186**: p. 1-10.
8. Hutchings, I., *Wear by particulates*. Chemical Engineering Science, 1987. **42**(4): p. 869-878.
9. Hutchings, I.M. and Shipway, P., *Tribology: Friction and Wear of Engineering Materials*. 2nd ed. 2017, London: Butterworth-Heinemann.
10. Efird, K.D., *Flow accelerated corrosion testing basics*, in CORROSION 2006. 2006, NACE International: San Diego, CA.
11. Nešić, S., Solvi, G.T., and Enerhaug, J., *Comparison of the Rotating Cylinder and Pipe Flow Tests for Flow-Sensitive Carbon Dioxide Corrosion*. Corrosion, 1995. **51**(10): p. 773-787.
12. Prozhega, M., Tatus, N., Samsonov, S., Kolyuzhni, O.Y., and Smirnov, N., *Experimental study of erosion-corrosion wear of materials: A review*. Journal of Friction and Wear, 2014. **35**(2): p. 155-160.
13. Clark, H.M. and Wong, K.K., *Impact angle, particle energy and mass loss in erosion by dilute slurries*. Wear, 1995. **186–187, Part 2**(0): p. 454-464.
14. Jiang, J., Xie, Y., Islam, M.A., and Stack, M., *The Effect of Dissolved Oxygen in Slurry on Erosion–Corrosion of En30B Steel*. Journal of Bio-and Triboro-Corrosion, 2017. **3**(4): p. 45.
15. Rajahram, S.S., Harvey, T.J., Walker, J.C., Wang, S.C., Wood, R.J.K., and Lalev, G., *A study on the evolution of surface and subsurface wear of UNS S31603 during erosion–corrosion*. Wear, 2011. **271**(9–10): p. 1302-1313.
16. Rajahram, S.S., Harvey, T.J., and Wood, R.J.K., *Evaluation of a semi-empirical model in predicting erosion–corrosion*. Wear, 2009. **267**(11): p. 1883-1893.

17. Barker, R., Hu, X., Neville, A., and Cushnaghan, S., *Inhibition of flow-induced corrosion and erosion-corrosion for carbon steel pipe work from an offshore oil and gas facility*. Corrosion, 2012. **69**(2): p. 193-203.
18. Gnanavelu, A., Kapur, N., Neville, A., and Flores, J.F., *An integrated methodology for predicting material wear rates due to erosion*. Wear, 2009. **267**(11): p. 1935-1944.
19. Hu, X., Alzawai, K., Gnanavelu, A., Neville, A., Wang, C., Crossland, A., and Martin, J., *Assessing the effect of corrosion inhibitor on erosion–corrosion of API-5L-X65 in multi-phase jet impingement conditions*. Wear, 2011. **271**(9–10): p. 1432-1437.
20. Hu, X., Barker, R., Neville, A., and Gnanavelu, A., *Case study on erosion–corrosion degradation of pipework located on an offshore oil and gas facility*. Wear, 2011. **271**(9): p. 1295-1301.
21. Hu, X. and Neville, A., *CO₂ erosion–corrosion of pipeline steel (API X65) in oil and gas conditions - A systematic approach*. Wear, 2009. **267**(11): p. 2027-2032.
22. Mansouri, A., Arabnejad, H., Shirazi, S.A., and McLaury, B.S., *A combined CFD/experimental methodology for erosion prediction*. Wear, 2015. **332–333**: p. 1090-1097.
23. Neville, A. and Wang, C., *Erosion–corrosion of engineering steels - Can it be managed by use of chemicals?* Wear, 2009. **267**(11): p. 2018-2026.
24. Neville, A. and Wang, C., *Erosion–corrosion mitigation by corrosion inhibitors—An assessment of mechanisms*. Wear, 2009. **267**(1–4): p. 195-203.
25. Wood, R.J.K., Puget, Y., Trethewey, K.R., and Stokes, K., *The performance of marine coatings and pipe materials under fluid-borne sand erosion*. Wear, 1998. **219**(1): p. 46-59.
26. Aribo, S., Barker, R., Hu, X., and Neville, A., *Erosion–corrosion behaviour of lean duplex stainless steels in 3.5% NaCl solution*. Wear, 2013. **302**(1): p. 1602-1608.
27. Senatore, E.V., Taleb, W., Owen, J., Hua, Y., Gomes, J.A.C.P., Barker, R., and Neville, A., *Evaluation of high shear inhibitor performance in CO₂-containing flow-induced corrosion and erosion-corrosion environments in the presence and absence of iron carbonate films*. Wear, 2018. **404-405**: p. 143-152.
28. Owen, J., Ramsey, C., Barker, R., and Neville, A., *Erosion-corrosion interactions of X65 carbon steel in aqueous CO₂ environments*. Wear, 2018. **414-415**: p. 376-389.
29. Vivar Mora, L., Taylor, A., Paul, S., Dawson, R., Wang, C., Taleb, W., Owen, J., Neville, A., and Barker, R., *Impact of silica nanoparticles on the morphology and mechanical properties of sol-gel derived coatings*. Surface and Coatings Technology, 2018. **342**: p. 48-56.
30. Gulbrandsen, E. and Grana, A., *Testing of Carbon Dioxide Corrosion Inhibitor Performance at High Flow Velocities in Jet Impingement Geometry. Effects of Mass Transfer and Flow Forces*. CORROSION, 2007. **63**(11): p. 1009-1020.
31. Efird, K., Wright, E., Boros, J., and Hailey, T., *Correlation of steel corrosion in pipe flow with jet impingement and rotating cylinder tests*. Corrosion, 1993. **49**(12): p. 992-1003.
32. Hassani, S., Roberts, K.P., Shirazi, S., Shadley, J.R., Rybicki, E.F., and Joia, C., *A New Approach for Predicting Inhibited Erosion-Corrosion in CO₂-Saturated Oil/Brine Flow Condition*. SPE Production & Operations, 2013. **28**(02): p. 135-144.
33. Hassani, S., Roberts, K.P., Shirazi, S.A., Shadley, J.R., Rybicki, E.F., and Joia, C., *Characterization and Prediction of Chemical Inhibition Performance for Erosion-*

- Corrosion Conditions in Sweet Oil and Gas Production.* Corrosion, 2012. **68**(10): p. 885-896.
34. Nassef, A.S., Banazadeh-Neishabouri, N., Keller, M.W., Roberts, K.P., Rybicki, E.F., Iski, E.V., and Shirazi, S.A. *Comparison of Erosion Resistance of Iron Carbonate Protective Layer with Calcium Carbonate Particles Versus Sand.* in *Abu Dhabi International Petroleum Exhibition & Conference.* 2017. Abu Dhabi: Society of Petroleum Engineers.
35. Nassef, A.S., Roberts, K.P., Rybicki, E.F., Keller, M.W., Iski, E.V., and Shirazi, S.A. *Comparison of Inhibited Erosion-Corrosion With Calcium Carbonate Particles Versus Sand.* in *CORROSION 2018.* 2018. Phoenix, AZ: NACE International.
36. Hassani, S., Roberts, K., Shirazi, S., Shadley, J., Rybicki, E., and Joia, C., *Flow loop study of NaCl concentration effect on erosion, corrosion, and erosion-corrosion of carbon steel in CO₂-saturated systems.* Corrosion, The Journal of Science and Engineering, 2012. **68**(2): p. 026001-1-026001-9.
37. Shadley, J.R., Shirazi, S.A., Dayalan, E., Ismail, M., and Rybicki, E.F., *Erosion-Corrosion of a Carbon Steel Elbow in a Carbon Dioxide Environment.* CORROSION, 1996. **52**(9): p. 714-723.
38. Shadley, J.R., Rybicki, E.F., Shirazi, S.A., and Dayalan, E., *Velocity Guidelines for Avoiding Erosion-Corrosion Damage in Sweet Production With Sand.* Journal of Energy Resources Technology, 1998. **120**(1): p. 78-83.
39. Zeng, L., Zhang, G., and Guo, X., *Erosion-corrosion at different locations of X65 carbon steel elbow.* Corrosion Science, 2014. **85**: p. 318-330.
40. Zeng, L., Zhang, G.A., Guo, X.P., and Chai, C.W., *Inhibition effect of thioureidoimidazoline inhibitor for the flow accelerated corrosion of an elbow.* Corrosion Science, 2015. **90**: p. 202-215.
41. Rincon, H., Shadley, J.R., and Rybicki, E.F. *Erosion Corrosion Phenomena of 13Cr at Low Sand Rate Levels.* in *CORROSION 2005.* 2005. NACE International.
42. Rincon, H., Shadley, J.R., Rybicki, E.F., and Roberts, K.P., *Erosion-Corrosion of Carbon Steel in CO₂ Saturated Multiphase Flows Containing Sand.* CORROSION 2006, 2006.
43. Owen, J.J. *Erosion-Corrosion of Carbon Steel in Complex Flow Geometries in Oil & Gas CO₂ Environments.* Ph.D. thesis, University of Leeds, 2018.
44. McLaury, B., Wang, J., Shirazi, S., Shadley, J., and Rybicki, E. *Solid particle erosion in long radius elbows and straight pipes.* in *SPE Annual Technical Conference and Exhibition.* 1997. San Antonio, TX: Society of Petroleum Engineers.
45. Ukpai, J.I., Barker, R., Hu, X., and Neville, A., *Exploring the erosive wear of X65 carbon steel by acoustic emission method.* Wear, 2013. **301**(1): p. 370-382.
46. Ukpai, J.I., Barker, R., Hu, X., and Neville, A., *Determination of particle impacts and impact energy in the erosion of X65 carbon steel using acoustic emission technique.* Tribology International, 2013. **65**(0): p. 161-170.
47. Ashby, M.F. and Jones, D.R.H., *Engineering materials 2: an introduction to microstructures, processing and design.* 3rd ed. 2005, London: Elsevier Butterworth-Heinemann.
48. Yunus, A.C. and Cimbala, J.M., *Fluid mechanics fundamentals and applications.* McGraw-Hill. 2006, Boston.
49. Chen, X., McLaury, B.S., and Shirazi, S.A., *Numerical and experimental investigation of the relative erosion severity between plugged tees and elbows in dilute gas/solid two-phase flow.* Wear, 2006. **261**(7-8): p. 715-729.